Biochimica et Biophysica Acta 1842 (2014) 2468–2478

Contents lists available at ScienceDirect

Biochimica et Biophysica Acta

journal homepage: www.elsevier.com/locate/bbadis

Mitochondrial apoptosis-inducing factor is involved in doxorubicin-induced toxicity on H9c2 cardiomyoblasts

Ana C. Moreira [a,b,1], Ana F. Branco [a,b,1], Susana F. Sampaio [a,b,1], Teresa Cunha-Oliveira [a], Tatiana R. Martins [a,b], Jon Holy [c], Paulo J. Oliveira [a,*], Vilma A. Sardão [a]

[a] CNC — Center for Neuroscience and Cell Biology, University of Coimbra, Portugal
[b] Department of Life Sciences, University of Coimbra, Portugal
[c] Department of Biomedical Sciences, University of Minnesota, Medical School-Duluth, Duluth, MN, USA

ARTICLE INFO

Article history:
Received 30 October 2013
Received in revised form 19 September 2014
Accepted 26 September 2014
Available online 2 October 2014

Keywords:
Doxorubicin
Apoptosis-inducing factor
Apoptosis
Cardiomyoblast

ABSTRACT

The cardiotoxicity induced by the anti-cancer doxorubicin involves increased oxidative stress, disruption of calcium homeostasis and activation of cardiomyocyte death. Nevertheless, antioxidants and caspase inhibitors often show little efficacy in preventing cell death. We hypothesize that a caspase-independent cell death mechanism with the release of the apoptosis-inducing factor from mitochondria is involved in doxorubicin toxicity. To test the hypothesis, H9c2 cardiomyoblasts were used as model for cardiac cells. Our results demonstrate that z-VAD-fmk, a pan-caspase inhibitor, does not prevent doxorubicin toxicity in this cell line. Doxorubicin treatment results in AIF translocation to the nuclei, as confirmed by Western Blotting of cell fractions and confocal microscopy. Also, doxorubicin treatment of H9c2 cardiomyoblasts resulted in the appearance of 50 kbp DNA fragments, a hallmark of apoptosis-inducing factor nuclear effects. Apoptosis-inducing factor knockdown using a small-interfering RNA approach in H9c2 cells resulted in a reduction of doxorubicin toxicity, including decreased p53 activation and poly-ADP-ribose-polymerase cleavage. Among the proteases that could be responsible for apoptosis-inducing factor cleavage, doxorubicin decreased calpain activity but increased cathepsin B activation, with inhibition of the latter partly decreasing doxorubicin toxicity. Altogether, the results support that apoptosis-inducing factor release is involved in doxorubicin-induced H9c2 cell death, which explains the limited ability of caspase inhibitors to prevent toxicity.

1. Introduction

Doxorubicin (DOX) is an anthracycline widely used for the treatment of different types of cancer [1]. The efficacy of DOX on tumor cells results from different mechanisms, including its ability to inhibit nuclear DNA replication [2–4] and its potential to generate oxygen radicals [5,6], ultimately resulting in cell death. Despite its effectiveness, DOX treatment often results in the development of chronic and cumulative cardiotoxicity, manifested as congestive heart failure [7]. The progressive and persistent character of DOX-induced cardiotoxicity can lead to cardiovascular alterations decades after treatment [8–10]. Cardiomyocyte apoptosis and consequent cell loss can be a mechanism by which DOX causes a deterioration of cardiac function, as described in different biological systems [11], although the extension and mechanisms are still unclear [7]. Both mitochondrial-dependent [12] and independent [13] signaling have been described in the context of DOX-induced cardiac cell death and the transcription factor p53 is apparently involved in up-stream events that lead to mitochondrial activation of the apoptotic pathway [14]. Despite several end-points for apoptosis are measured in cells treated with DOX, the appearance of apoptotic/necrotic cardiomyocytes, as characterized from a morphological point of view, appears to be low when evaluated in post-mortem samples of cardiac tissue from patients [15]. Nevertheless, confounding factors including a peak of apoptotic induction in cardiac cells occurring early in the treatment and thus not detected *post-mortem* [16] or masquerading fibrosis [17] may occur. One interesting feature of DOX-induced cell death in several systems is the fact that caspase-inhibitors are not fully protective, which has been confirmed by the fact that DOX-induced cell death can follow caspase-independent signaling pathways [18].

The objective of this work was to find out if the apoptosis-inducing factor (AIF) is released from mitochondria during DOX treatment and whether it plays any relevant role in cell death signaling. AIF is a flavoprotein consisting of three structural components: a FAD-binding

Abbreviations: AIF, apoptosis-inducing factor; $\Delta\Psi$, mitochondrial transmembrane electric potential; DOX, doxorubicin; LDH, lactate dehydrogenase; OT4, On TargetPlus scrambled negative control; PARP, Poly ADP ribose polymerase; PFGE, Pulse-field Gel Electrophoresis; siRNA, small-interfering RNA; SRB, sulforhodamine B

* Corresponding author at: Center for Neuroscience and Cell Biology, Largo Marquês de Pombal, University of Coimbra, 3004-517 Coimbra, Portugal. Tel.: +351 304 502911; fax: +351 239 853409.
E-mail address: pauloliv@ci.uc.pt (P.J. Oliveira).

[1] These authors contributed equally to this manuscript.

http://dx.doi.org/10.1016/j.bbadis.2014.09.015
0925-4439/

domain, a NAD-binding domain and a C-terminal domain, which plays a role in apoptosis. The AIF has NADH oxidase activity and is normally located within the mitochondrial intermembrane space or loosely associated with the inner mitochondrial membrane [19,20]. The AIF mature form (57 kDa) is released into the cytoplasm through rupture of the outer membrane associated with the permeability transition [21] or through pores formed by the pro-apoptotic Bcl-2 family members Bax, Bak, and Bid [22]. Poly (ADP-ribose) polymerase-1 (PARP-1) is also involved in AIF translocation from mitochondria to the nucleus [23,24], triggering chromatin condensation and large-scale DNA fragmentation in a caspase-independent mechanism. The fact that AIF apoptogenic effects are not eliminated in the presence of the pan-caspase inhibitor benzyloxycarbonyl-Val-Ala-Asp (OMe) fluoromethylketone (z-VAD-fmk) suggests that AIF signaling is independent of caspase activation [12]. In order to test our hypothesis, the cardiomyoblast cell line H9c2 was used in the present study. This cell line, derived from rat myocardium, is widely recognized as an *in vitro* model to study DOX-induced biochemical and morphological changes [12,25,26], as well as the effects of several potential protective compounds [27–29]. We have previously shown that DOX induces mitochondrial depolarization and phosphatidylserine externalization [27], as well as activation of the p53/Bax axis [14,30].

Previous results suggested the hypothesis that DOX cardiotoxicity on H9c2 cardiomyoblasts involves AIF release: a) DOX generates oxidative stress that promotes AIF proteolysis [6,14], b) DOX activates calpains in cardiac cells [31,32], possibly as a result of calcium overloading [14] and c) DOX-induced cell death is not completely inhibited by caspase inhibitors, suggesting also the involvement of a caspase-independent cell death [18].

Due to the clinical relevance of DOX as an effective anti-cancer agent, a full understanding of how it induces cell damage and death are paramount to designing effective protective strategies to reduce its toxic side effects on the cardiovascular system.

2. Materials and methods

2.1. Reagents

Dulbecco's modified Eagle's medium (DMEM), penicillin, streptomycin, fetal bovine serum (FBS) and Trypsin were purchased from Gibco-Invitrogen (Grand Island, NY, USA). Doxorubicin, dithiothreitol (DTT), phenylmethanesulfonyl fluoride (PMSF), protease inhibitor cocktail (leupeptin, antipain, chymostatin, and pepstatin A), sulforhodamine B (SRB) were obtained from Sigma (St. Louis, USA). Hoechst 33342, tetramethylrhodamine methyl ester (TMRM), and Mitotracker Red CMXROS were obtained from Invitrogen/Molecular Probes (Eugene, OR, USA). Rabbit anti-AIF (1:1000), rabbit anti-GADPH (1:1000), rabbit anti-COXIV (1:1000), rabbit anti-Lamin A/C and mouse anti-p53 (1:1000) were obtained from Cell Signaling (Danvers, MA, USA); rabbit anti-PARP (1:1000) was purchased from Santa Cruz (Santa Cruz, CA, USA). Secondary antibody Fluorescein (FITC) anti-Mouse IgG and alkaline phosphatase (AP)-conjugated were purchased from Jackson ImmunoResearch Laboratories, Inc. (Cambridgeshire, UK). Caspase substrate (Ac-DEVD-pNA) was purchased from Calbiochem (San Diego, CA, USA). z-VAD-fmk was obtained from Alexis (Farmingdale, NY, USA) and ethidium bromide was obtained from Bio-Rad (Hercules, CA, USA). Lipofectamine® 2000 Transfection Reagent was purchased from Invitrogen (Carlsbad, CA, USA). Opti-MEM® I Reduced Serum Medium was purchased from Gibco (Rockville, MD, USA). 5× siRNA buffer was obtained from Dharmacon — Thermo Scientific (Waltham, MA, USA). AIF siRNA (Rn_Pdcd8_1) was obtained from Qiagen (Germantown, MD, USA). The MDL28170 inhibitor was kindly provided by Dr Inês Araújo from the University of Algarve, Portugal. The cathepsin B inhibitor CA-074 Me was from Enzo Life Sciences (Farmingdale, NY, USA). DOX was dissolved in milli-Q water at a stock solution of 25 mM.

2.2. Cell culture and treatments

The H9c2 cell line was purchased from American Tissue Type Collection (Manassas, VA; Catalog # CRL – 1446). Cells were cultured in DMEM medium supplemented with 1.5 g/l sodium bicarbonate, 10% fetal bovine serum, 100 U/ml of penicillin and 100 μg/ml of streptomycin in 150 cm^2 tissue culture flasks at 37 °C in a humidified atmosphere of 5% CO_2. Cells were treated with 0.5 and 1 μM DOX for 6, 24 or 48 h, according to the assay. These DOX concentrations are clinically relevant, as they fall well within the concentrations of DOX found in the plasma of patients undergoing DOX therapy [33]. The experiments performed in the presence of z-VAD-fmk, the compound was added to the cells in a concentration of 50 μM, 1 h prior to DOX treatment. The calpain inhibitor MDL28170 and the cathepsin B inhibitor CA-074 Me were added 30 or 90 min before DOX treatment, respectively, at a concentration of 10 μM. For immunocytochemistry, cells were seeded on glass coverslips at a density of 3.5×10^4 cells/ml in six well plates containing coverslips (final volume of 2 ml per well). For sulforhodamine B assay, cells were also seeded at 3.5×10^4 cells/ml in 24 well-plates at a final volume of 1 ml per well.

2.3. Cytotoxicity and cell density evaluation by sulforhodamine B (SRB) assay

The sulforhodamine B (SRB) assay, a colorimetric method used for cell density determination, is based on the measurement of cellular protein mass [34]. H9c2 cells (3.5×10^4 cells/ml) were seeded in 24 well-plates and at specific time points, the incubation media was removed and cells were fixed with ice-cold methanol containing 1% acetic acid for at least 30 min. Cells were then incubated with 0.5% (wt/vol) SRB dissolved in 1% acetic acid for 1 h at 37 °C. The unbound dye was removed with 1% acetic acid solution. Dye bound to cell proteins was extracted with 10 mM Tris-base solution, pH 10, and the optical density determined at 540 nm. Results were expressed as a percentage of time zero (first time point harvested after cell attachment, 24 h after seeding).

2.4. Metabolic cell viability assessment through the resazurin reduction assay

H9c2 cells were seeded at a density of 87,500 cells/ml for 6 hour treatments or at a density of 35,000 cells/ml for 24 and 48 hour treatments in 96-well plates. After 24 h of cell attachment, H9c2 cells were incubated for 6, 24 and 48 h with 0.5 and 1 μM DOX. At the end of the treatment, the culture medium was removed and cells were incubated for 40 min with 75 μl of culture medium supplemented with 10 μg/ml resazurin. The amount of resazurin reduced to resorufin, indicative of metabolic activity, was measured fluorimetrically with 570 nm excitation and 600 nm emission in Biotek Cytation 3 reader (Biotek Instruments, Winooski, VT, USA).

2.5. Collection of total, cytosolic, mitochondrial and nuclear extracts from H9c2 cells

To obtain total cellular extracts, H9c2 cells were harvested by trypsinization after treatments and washed once with PBS. In order to collect total cells (attached and floating dead cells), two centrifugation steps were performed for 5 min at 1000 ×*g*. The cellular pellet was resuspended in collecting buffer (20 mM HEPES/NaOH, pH 7.5, 250 mM Sucrose, 10 mM KCl, 2 mM $MgCl_2$, 1 mM EDTA) supplemented with 2 mM dithiothreitol (DTT), 100 μM phenylmethylsulfonyl fluoride (PMSF) and a protease inhibitor cocktail (containing 1 μg/ml of leupeptin, antipain, chymostatin and pepstatin A) and ruptured by 30 passages through a 27-gauge needle. The cell suspension was then kept at −80 °C until used. For subcellular fractionation, cells were harvested as described above and resuspended in homogenization buffer (250 mM sucrose, 20 mM K^+ Hepes pH 7.5, 10 mM KCl, 1.5 mM

$MgCl_2$, 0.1 mM EDTA, 1 mM EGTA) supplemented with 1 mM DTT, 100 μM PMSF and protease inhibitor cocktail (containing 1 μg/ml of leupeptin, antipain, chymostatin and pepstatin A). Cells were incubated in homogenization buffer for 15 min on ice. Cells were then transferred to a pre-cooled tissue homogenizer and homogenized 30 times using a tight pestle. The homogenized cells were centrifuged at 217 ×*g* for 5 min at 4 °C. The pellet was discarded and the supernatant was centrifuged again at 14,000 ×*g* for 15 min at 4 °C. The pellet, containing the mitochondrial fraction was resuspended in 50 μl of homogenization buffer. Mitochondrial fractions were stored at −80 °C until used. For cytosolic and nuclear extraction, the K266-100 Nuclear/Cytosol Fractionation kit from Biovision (Milpitas, CA, USA) was used. Specific protein markers for each fraction were tested to evaluate their purity. Protein contents were determined using the Bradford assay with bovine serum albumin as standard.

2.6. Western Blot analysis

After denaturation at 95 °C for 5 min in a Laemmli buffer (from Bio-rad), equivalent amounts of proteins (25 μg) were separated by electrophoresis in 8% or 12% SDS-polyacrylamide gels (SDS-PAGE) and electrophoretically transferred to a polyvinylidene difluoride (PVDF) membrane for 90 min at 100 V. After blocking membranes with 5% milk in TBST (50 mM Tris-HCl, pH 8; 154 mM NaCl and 0.1% Tween 20) for 2 h at room temperature, membranes were incubated overnight at 4 °C with the respective antibodies: rabbit anti-AIF (1:1000), rabbit anti-GADPH (1:1000), rabbit anti-COXIV (1:1000), rabbit anti-Lamin A/C (1:1000), mouse anti-p53 (1:1000) and rabbit anti-PARP (1:1000). Membranes were washed and incubated with the secondary goat anti-mouse IgG (1:2500) and goat anti-rabbit IgG (1:2500) antibodies. Membranes were then incubated with the ECF detection system (GE Healthcare, Piscataway, NJ) and imaged with Versa Doc imaging system (Bio-Rad, Hercules, CA). Densities of each band were calculated with Quantity One Software (Bio-Rad). Membranes were also stained with Ponceau reagent from Bio-Rad (Hercules, CA, USA) to confirm equal protein loading in each lane. This experimental strategy was preferred over the use of housekeeping proteins (such as actin or other protein) since their expression can be altered after DOX treatment.

2.7. Double fluorescence imaging of H9c2 cells with TMRM and Hoecshst 33342

H9c2 cells were treated as previously described in this section and then incubated with $TMRM^+$ (100 nM), Hoechst (1 μg/μl), 30 min at 37 °C in the dark. Cells were observed under a Zeiss LSM 510 Meta confocal microscope. A lower concentration of $TMRM^+$ was maintained in the media in order to avoid leakage from mitochondria. Images were obtained through LSM Image Browser.

2.8. Immunocytochemistry

Cells were seeded on glass coverslips in 6-well plates, at a density of 35,000 cells/ml. Doxorubicin (0.5 μM and 1 μM) was incubated with cells for 24 and 48 h. After the end of the treatment, cells were incubated with Mitotracker Red (125 nM) for 30 min at 37 °C in the dark, washed twice with cold PBS and fixed with 100% ice-cold methanol overnight at −20 °C. Cells were washed/rehydrated 3 times with PBST (PBS supplemented with 0.1% Tween-20) during 5 min. Cells were then incubated with blocking solution (PBST supplemented with1% BSA) for 1 h at room temperature. Cells were incubated with a primary antibody (anti-AIF, 1:100 in blocking solution) overnight and stained with FITC-secondary antibody (goat anti-mouse, 1:50 in blocking solution), supplemented with 1 μl/ml of Hoechst 33342, during 2 h at room temperature. Between incubations with the primary and secondary antibodies, cells were rinsed 3 times with PBS-T during 5 min each. Coverslips were mounted on glass slides. Cells were observed under a Zeiss LSM 510Meta confocal microscope with the LSM Image Browser software.

2.9. Caspase-3-like colorimetric activity assay

Total cellular extracts were collected by trypsinization and centrifuged twice at 1000 ×*g*, 4 °C during 5 min. Floating cells were also collected. The pellet was resuspended in collecting buffer (20 mM HEPES/NaOH pH 7.5, 250 mM Sucrose, 10 mM KCl, 2 mM $MgCl_2$, 1 mM EDTA) supplemented with 2 mM DTT, 100 μM phenylmethylsulfonyl fluoride (PMSF) and a protease inhibitor cocktail, containing 1 μg/ml of leupeptin, antipain, chymostatin and pepstatin A. Protein contents were determined by the Bradford assay. To measure caspase 3-like activity, aliquots of cell extracts containing 25 μg of protein were incubated in the reaction buffer, containing 25 mM Hepes (pH = 7.5), 10% sucrose, 10 mM DTT, 0.1% CHAPS and 100 μM caspases substrate Ac-DEVD-pNA for 2 h at 37 °C. Caspases-like activity was determined by following the detection of the chromophore p-nitroanilide after cleavage from labeled substrate Ac-DEVD. The method was calibrated with known concentrations of p-nitroanilide (pNA) and the results are expressed as amount of pNA released (nM)/μg of protein.

2.10. Pulse field-gel electrophoresis

In order to detect large scale DNA fragmentation, Pulse Field-Gel Electrophoresis (PFGE) was performed. Cells were harvested by trypsinization and centrifuged. The pellet was washed once with ice cold PBS containing 5 mM of EDTA (PBS/EDTA) and counted with a hemocytometer. Suspension containing $2–3 \times 10^5$ cells was transferred for a new 15 ml conical tube and centrifuged again. The supernatant was removed and cells were mix with Low Gelling Temperature (LGT) embedding solution (0.1 ml of 1 M Tris-HCl (pH 7.5), 2 ml of 0.5 M EDTA, 0.1 g of LGT agarose, 0.5% Triton-X 100 and 10 g/ml of RNAse). Immediately, the cell/agarose mix was transferred to plug mold and chilled at 4 °C for 10–20 min. The agarose chip was transferred to a 2 ml centrifuge tube containing 1 ml of 10 mM Tris, pH7.5, 0.1 M EDTA, 0.2% Triton X-100 and 10 l of 20 mg/ml proteinase K. The samples were incubated overnight in a dry block at 50 °C. The agarose chip was washed in TBE (40 mM Tris; 40 mM Boric Acid; 1 mM EDTA) for 3 times during 10 min each. One % agarose gel was then prepared and casted in TBE. While the gel was polymerizing, the TBE running buffer was added to PFGE apparatus and chips were loaded into wells, with PFGE markers (0.1–200 kbp Sigma, St Louis, USA) being included as well. The wells were then filled with LGT agarose and the running started after 10 min with the following settings: initial time: 5 s; final time: 120 s; run time 24 h; voltage: 150 V (CHEF DR-II system, from Bio-Rad). At the end of the run, agarose gel was stained with ethidium bromide during 30 min, washed and visualized under UV light.

2.11. siRNA-mediated knockdown of the AIF in H9c2 cells

In the day prior to transfection, cells were plated in 60 mm-diameter plates at a density of 35,000 cells/ml in DMEM. Cells were approximately 60% confluent prior to transfection. On the day of transfection, cells were incubated with AIF small interfering RNA (siRNA) (Qiagen, catalog number SI03025379/Rn_Pdcd8_1, sequence: TTGGGTCGAAGGAGAGTAGAA), with On TargetPlus scrambled negative control (OT4, scrambled RNA) (Dharmacon, catalog number #11811994, sequence: UGGUUUACAUGUUUUCCUA) or with RNA buffer solution (negative control). In one tube, 6.7 μl/plate of siRNA against AIF mRNA or OT4 mRNA were diluted in Opti-MEM and siRNA buffer solution; in a separate tube, 6 μl/plate of Lipofectamine was diluted in 500 μl/plate of Opti-MEM. Both tubes were incubated for 5 min at room temperature, following which the two tubes (siRNA AIF with Lipofectamine or siRNA OT4 with Lipofectamine) were mixed together and incubated for another

20 min at room temperature to allow for the formation of transfection complexes. Plates were washed three times with PBS and filled with 1.5 ml of Opti-MEM. One milliliter aliquot of the solution was then added to each plate and gently mixed to ensure uniform distribution. The plates were then incubated at 37 °C humidified atmosphere containing 5% CO_2 and 95% air for 5 h. Following this incubation, 2.5 ml of DMEM was added. The media were again changed to fresh DMEM after 24 h and cells were treated with DOX for the required experimental protocol.

2.12. Lactate dehydrogenase (LDH) release assay

After incubation with DOX, the medium was collected from wells, centrifuged at 18,000 ×*g* (Eppendorf 5415C) during 10 min at 4 °C and the supernatant stored in new microtube and kept at −80 °C. To measure LDH enzymatic activity, the samples were incubated with a pyruvate (Tris 81.3 mM, NaCl 203.3 mM, Pyruvate 9.76 mM) and NADH-containing reaction media (Tris 81.3 mM, NaCl 203.3 nM, NADH 0.244 mM) and readily read at 340 nm. Blanks were done in a reaction media lacking pyruvate and the rate of absorbance decrease was obtained. Values were presented as % of control.

2.13. Calpain activity assay

H9c2 cells were seeded at a density of 87,500 cells/ml for 6 h treatments and at 35,000 cells/ml for 24 and 48 hour treatments, in 96-well plates. After 24 h of cell attachment, H9c2 cells were incubated for 6, 24 and 48 h with 0.5 and 1 μM DOX. After the treatment, cells were lysed with 0.9% Triton X-100. Protein contents were determined by the Bradford method. The CalpainGLO luciferase detection reagent from the Calpain Glo protease assay (Promega) was then added in a 1:1 proportion to the cellular extracts, incubated for 15 min and the luminescence was detected in a Biotek Cytation 3 reader (Biotek Instruments, Winooski, VT, USA).

2.14. Cathepsin activity assay

H9c2 cells were seeded at a density of 35,000 cells/ml concentration in a total volume of 10 ml at 100 mm diameter dishes. After 48 h of cell attachment, H9c2 cells were incubated for 24 h with 1 DOX. Following the treatment, culture media was collected and was added 3 ml of extraction buffer (PBS supplemented with 0.1 g/L of EDTA) to each dish. Cells were then scraped and the cell suspension was collected and added to the correspondent culture medium. The suspensions were centrifuged at 340 ×*g* rpm for 4 min, the pellet was collected and washed with PBS and centrifuged again at 340 ×*g* for 4 min. Pellets were ressuspended in 200 μl of Lysis Buffer (50 mM HEPES pH 7.4, 100 mM NaCl, 0.1% (wt/vol) CHAPS, 0.1 mM EDTA and 10 mM DTT). The cell suspensions were kept at −80 °C until used. The protein content was quantified by the Bradford method. Aliquots of 50 μl of each sample were incubated with 40 μM of z-Arg-Arg-N-methyl-coumarin in Incubation Buffer (100 mM Sodium Acetate pH 5.5, 1 mM EDTA, 5 mM DTT and 0.1% Brij-35) at 37 °C for 20 min. After the incubation, 150 μl of Stopping Buffer (33 mM Sodium Acetate pH 4.3, 33 mM Sodium Chloroacetate) were used to stop the enzymatic reaction. Cathepsin-B like activity was determined by the detection of the N-methyl-coumarin fluorimetrically with 360 nm excitation and 460 nm emission. The assay was calibrated with known concentrations of N-methyl-coumarin.

2.15. Statistical analysis

Data analysis was performed by using GraphPad Prism 6.0 program (GraphPad Software, Inc., La Jolla, CA, USA) and data were expressed as means ± SEM for the number of experiments indicated in the legends of the figures. Multiple comparisons were performed using one-way analysis of variance (ANOVA) followed by Bonferroni multiple comparison post-hoc test. Comparisons between two groups were performed by using a Student's *t*-test. Significance was accepted when p value < 0.05.

3. Results

3.1. Doxorubicin induces caspase-independent cell death

Caspase-dependent cell death has been reported to be involved in the cardiotoxicity associated with DOX therapy [11,35]. To test whether DOX-induced cell death is prevented by blocking caspase activity, z-VAD-fmk, a synthetic peptide that irreversibly inhibits caspase activity was used (Fig. 1). H9c2 cells were pre-incubated with 50 μM z-VAD-fmk for 1 h, followed by treatment with 1 μM DOX for 48 h. The decrease in H9c2 cell mass due to DOX-induced toxicity and the effect of a non-toxic z-VAD-fmk concentration was analyzed through the SRB dye-binding assay [34]. Our results demonstrate that z-VAD-fmk did not inhibit DOX-induced toxicity on H9c2 myoblasts (Fig. 1A), confirming previous studies [36]. The lack of protection by z-VAD-fmk on DOX toxicity was further confirmed using vital epifluorescence microscopy, in cells incubated with the mitochondrial probe TMRM and nuclear label Hoechst 33342 (Fig. 1B). The images obtained show that 1 μM DOX caused mitochondrial depolarization and a decrease in nuclear size, regardless of the presence of z-VAD-fmk, when incubated for 48 h. In order to confirm whether z-VAD-fmk incubation leads indeed to caspase inhibition, caspase-like activity was measured by using a colorimetric assay (Fig. 1C). As previously reported, DOX induced an increase in caspase-3-like activity in H9c2 myoblasts [14,27], even after 48 h of treatment (Fig. 1C). However, caspase inhibition by 50 μM z-VAD-fmk, when pre-incubated for 1 h before DOX treatment did not prevent DOX-induced decreased cell mass (Fig. 1A and B) although the same z-VAD-fmk concentration and treatment time inhibited DOX-induced caspase 3-like activity increase, showing that the inhibitor worked as expected. The results demonstrate that z-VAD-fmk inhibits DOX-induced caspase 3 activation but not the loss of cells (Fig. 1C).

3.2. Doxorubicin triggers large scale DNA fragmentation

Nuclear DNA fragmentation is a hallmark of apoptosis, generally orchestrated by caspases and normally used as an end-point for programmed cell death [37]. In some cell types, internucleosomal cleavage during apoptosis generates a characteristic 200 bp ladder; however, in most cells, however, 50 kbp or larger fragments are generated, in some instances preceding the subsequent formation of 200 bp fragments. H9c2 cell death induced by a 24 hour treatment with 1 μM DOX was not accompanied by 200 bp DNA laddering (data not shown); therefore, pulse-field gel electrophoresis (PFGE) was employed to test for large scale DNA cleavage. Treatment of H9c2 cells with 0.5 and 1 μM DOX resulted in the appearance of 50 kbp DNA fragments in H9c2 cells after 24 h of treatment, and more markedly after 48 h (Fig. 2A), which suggests involvement of AIF nuclear translocation [38].

3.3. Doxorubicin treatment results in AIF release and nuclear translocation

The inability of z-VAD-fmk to inhibit DOX-induced cell death, along with the appearance of large-scale DNA fragmentation, raised the possibility that AIF could be playing a determinant role in H9c2 responses to DOX. Previous studies have shown that apoptotic insults resulting in outer mitochondrial membrane permeabilization release AIF, which is subsequently translocated to the nucleus and serves as a pro-apoptotic stimulus [19]. To test whether AIF was released from mitochondria and translocated to the nucleus after DOX treatment, AIF content was evaluated in mitochondrial, cytosolic and nuclear

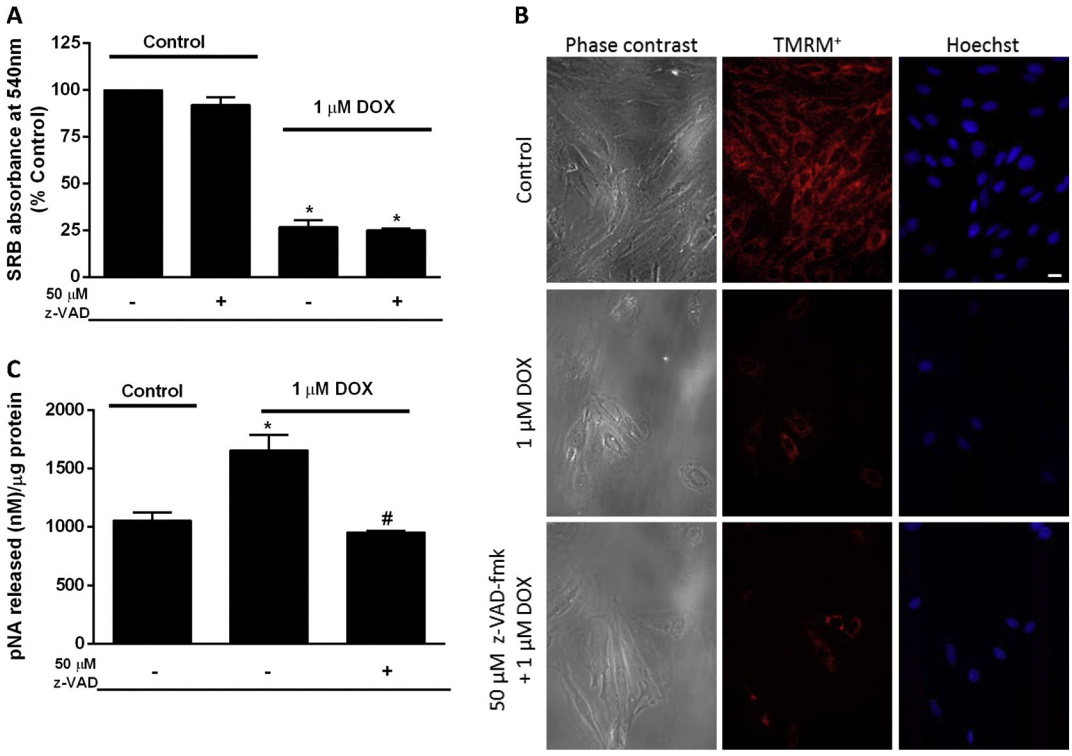

Fig. 1. Cytotoxicity of DOX is not completely prevented by the pan-caspase inhibitor z-VAD-fmk. The cytotoxicity of DOX on H9c2 myoblasts was analyzed in the presence or absence of the caspase inhibitor z-VAD-fmk by using the SRB technique (A) and vital epifluorescence microcopy (B). Arrows indicate nuclei with more condensed morphology after DOX treatment Panel C shows that z-VAD-fmk prevents DOX-induced caspase-3 activation in H9c2 cardiomyoblasts. Data represent mean ± SEM of 3–4 independent experiments, $^{*}p < 0.05$ compared with non-treated cells, $^{\#}p < 0.05$ compared with DOX-treated cells. Images in panel B are representative of 2 independent experiments. White bar represents 100 μm.

fractions by Western Blot and immunocytochemistry (Fig. 2B–F). After 48 hour treatment with 1 μM DOX, a decrease in the amount of AIF in mitochondrial fractions (Fig. 3D), and an increase in the cytosolic (Fig. 2E) and nuclear (Fig. 2F) fractions were observed. Whole cell extracts did not show any changes in total AIF content (Fig. 2C), indicating that AIF subcellular location, but not its overall quantity, was altered by DOX treatment. Three distinct markers were used to verify the purity of each fraction (Supplementary Fig. S1). The complex IV subunit, COX IV was used as mitochondrial marker, while glyceraldehyde 3-phosphate dehydrogenase (GAPDH) and lamin A/C were assessed as cytosolic and nuclear markers, respectively. The same proteins were present in the respective fractions as loading controls.

The release of AIF to the cytosol and its translocation to the nucleus was further confirmed by imunocytochemistry (Fig. 2B). In untreated H9c2 myoblasts, AIF protein was mostly located in mitochondria, co-localizing with the mitochondrial probe MitoTracker Red. However, upon DOX treatment, AIF fluorescence lost its preferential mitochondrial distribution, being detected in the nucleus after 48 hour treatment with 0.5 and 1 μM DOX.

3.4. AIF knockdown decreases doxorubicin-induced toxicity on H9c2 cells

The next experimental question regarded whether AIF downregulation could decrease DOX toxicity in H9c2 cells. For this purpose, the effects of DOX on naïve untransfected H9c2 cells, control H9c2 cells transfected with a non-target RNA (OT4), or H9c2 cells transfected with small interfering RNA targeting AIF mRNA (siRNA AIF) were compared. Using this knockdown protocol, AIF protein levels were reduced to 10–20% of basal levels (Fig. 3A). Twenty-four hours after transfection, cells were incubated with 1 μM of DOX for 24 and 48 h. Similar to previous experiments, a reduction in cell number – reflecting cell death – was observed in naive and control OT4-transfected cells after treatment with 1 μM DOX for both 24 (data not shown) and 48 h (Fig. 3B). In contrast, DOX-induced cell death was significantly inhibited in siRNA AIF knockdown cells, as demonstrated by the SRB (Fig. 3B) and lactate dehydrogenase (LDH) release assays (Fig. 3C). According to the SRB assay, an increase in cell mass was observed after DOX treatment in AIF knockdown cells, when compared with control and OT4-treated cells (Fig. 3B). Supporting results were also observed by performing the LDH release assay, where only AIF knockdown cells showed no significant increase in LDH release after 1 μM DOX treatment for 48 h (Fig. 3C). Previously, we found that H9c2 cells treatment with DOX resulted in an up-regulation of the transcription factor p53 [14]. We hypothesized at that time that nuclear DOX accumulation results in DNA damage and p53 activation, up-regulating Bax expression and causing its mitochondrial translocation, with consequent activation of the intrinsic apoptosis pathway [14]. When caspases are involved in cell death, PARP-1 cleavage and inactivation by those proteins drives the cell towards a point of no return [39]. Facing this, our next experimental question was whether AIF knockdown would decrease the cellular contents on p53 and PARP cleaved product, an 89 kDa protein fragment. Western Blotting was used to quantify p53 and full-length/cleaved PARP protein after treatment with 1 μM DOX for 48 h (Fig. 4). The results regarding p53 confirmed that DOX causes an increased content in that transcription factor in both control and OT4-treated cells. Interestingly, AIF knockdown decreased the effects of DOX on p53 content.

As observed in Fig. 4, the band corresponding to PARP full length (116 kDa) decreases upon DOX treatment (1 μM for 48 h) in all of the three cellular groups tested, in opposition with the cleaved 89 kDa form. However, and in agreement with previous results, the amount of cleaved PARP was higher in control or OT4 transfected cells than in AIF siRNA cells treated with DOX (Fig. 4C).

So far, the results suggest that DOX-induced cardiomyoblast cell death is mediated by AIF release. Thus, we investigated which proteases could be responsible for AIF cleavage, an initial step that would lead to its release. Since DOX was previously shown to increase intracellular calcium [14], and activate calpains in cardiac cells [31,32], we investigated the role of these calcium-activated proteases by studying the effect of

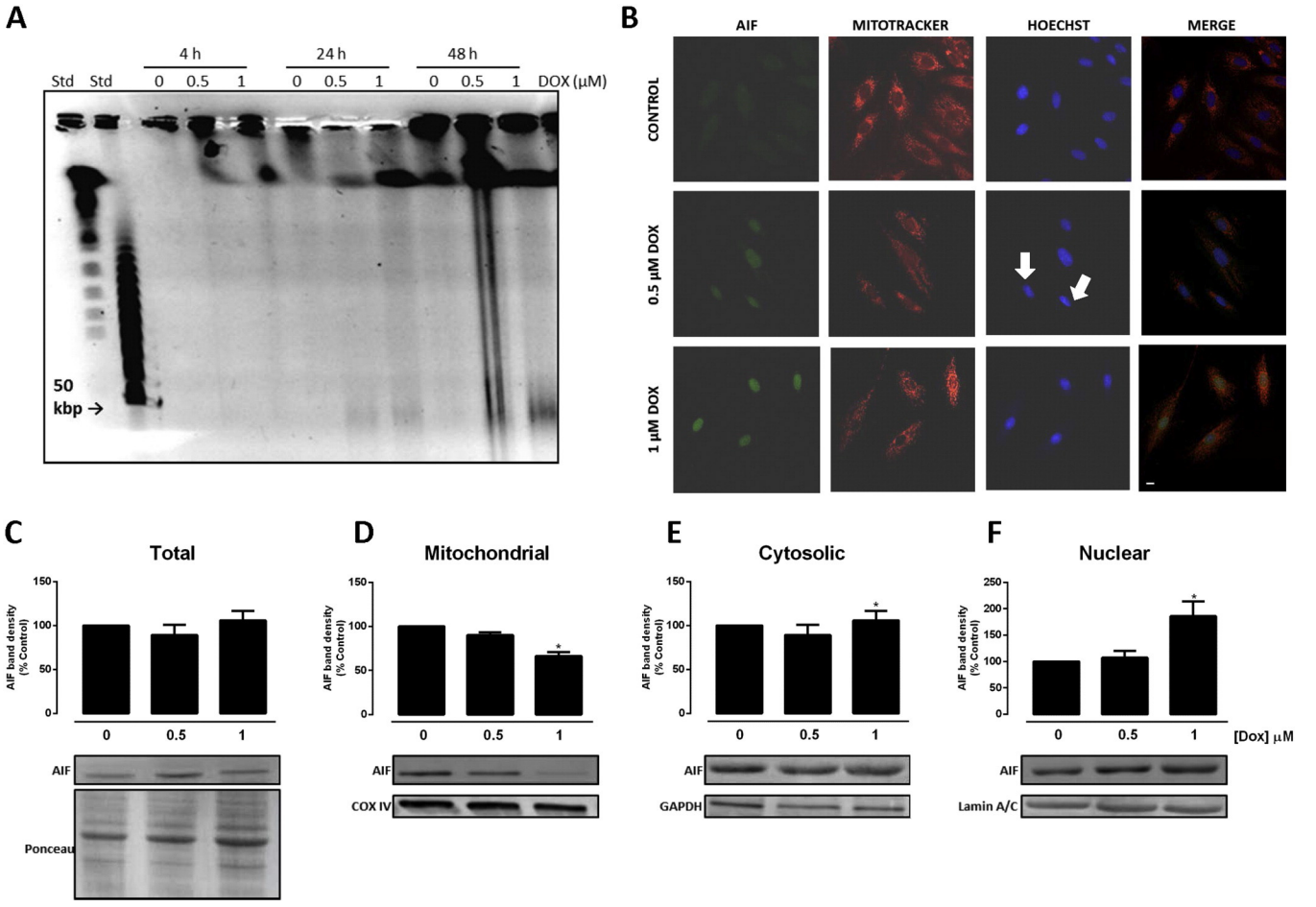

Fig. 2. DOX induces large scale DNA fragmentation and AIF translocation from mitochondria to the nucleus. A) DNA fragmentation in 50 kbp occurs 48 h treatment with DOX in the H9c2 cell line. This phenotype of DNA cleavage is a hallmark of AIF-induced fragmentation. The image is representative of two independent experiments. B) Laser confocal scanning imaging showing triple labeling with Hoechst 33342 (blue), immunostaining with AIF (green) and Mitotracker Red CMXROS (red) of untreated cells compared with cells treated with 0.5 μM or 1 μM DOX during 48 h. The results confirm AIF translocation to the nucleus. Images are representative of three different cell preparations. White bar represents 100 μm. C–F) Western Blot analysis of total, mitochondrial, cytosolic and nuclear extracts shows that (C) total AIF content does not change during the treatment; (D) treatment with DOX induces a decrease of mitochondrial AIF content and an increase in cytosolic and nuclear AIF content (E, F, respectively). Ponceau staining, COX IV, GADPH and Lamin A/C show an equal loading amount of protein in each lane. Graphs represent the densitometry analysis of AIF protein in each extract, expressed as % of control. Data represents mean ± SEM of four independent experiments $^{*}p < 0.05$, when compared with control (no DOX added).

the inhibitor MDL28170 on metabolic cell viability in H9c2 cells (Fig. 5). DOX significantly decreased metabolic cell viability after 24 and 48 h. (Fig. 5A). However, despite the increase in basal metabolic viability after 24 h and 48 h incubation with the inhibitor, no protection was observed against DOX toxicity (Fig. 5A). In fact, DOX induced a decrease in calpain activity after 24 and 48 h exposure (Fig. 5B), in agreement with recent reports [40]. Thus, we investigated the role of cathepsin B, which was previously shown to be activated by DOX in HeLa cells [41]. In our conditions, the cathepsin B inhibitor CA-074 Me partially protected against DOX toxicity (Fig. 5C), at a time point when DOX induced an increase in cathepsin B activity (Fig. 5D). These results support the idea that cathepsin B could be responsible by the cleavage of AIF that precedes its release from the mitochondria. Cathepsin D activity was not altered by DOX treatment (data not shown).

4. Discussion

Several mechanisms are proposed to explain the cardiotoxicity induced by DOX, such as the generation of reactive oxygen species [42], disruption of calcium homeostasis [43], disturbance of cardiac mitochondrial bioenergetics [28], and activation of p53/Bax pathway [14] followed by cell death through activation of caspase-dependent signaling [11]. Cell death in DOX-treated cells may also result from GATA-4 depletion [44], a transcriptional factor that regulates the apoptotic pathway by activating the antiapoptotic gene Bcl-X_L [45]. The use of caspase inhibitors to decrease DOX-induced cardiac damage is often ineffective, suggesting that DOX-induced cardiac cell death may occur through both caspase-independent and caspase-dependent pathways [18].

Caspase-independent cell death pathways can involve the mitochondrial release of AIF, a flavoprotein with NADH oxidase activity, located in the mitochondrial intermembrane space. The AIF was first identified as a pro-apoptotic protein, inducing caspase-independent cell death, involving chromatin condensation and large-scale DNA fragmentation [19]. It is noteworthy that the AIF is also involved in the maintenance and maturation of mitochondrial respiratory complex I, as well as peroxide scavenging activities [46], demonstrating a physiological role for that protein. Despite this, the apparent viability in our AIF siRNA H9c2 cell model was not altered (Fig. 3B). Regarding the pro-apoptotic role of AIF, the basic mechanism involves its release from the mitochondrial intermembrane space to the cytosol, followed by nuclear translocation. Once in the nucleus, AIF binds to nuclear DNA inducing chromatin condensation and large-scale DNA fragmentation. The nuclear effects resulting from AIF translocation require a direct interaction between AIF and DNA [47]. Cytosolic AIF also promotes a decrease in mitochondrial $\Delta\Psi$ and facilitates release of cytochrome *c*

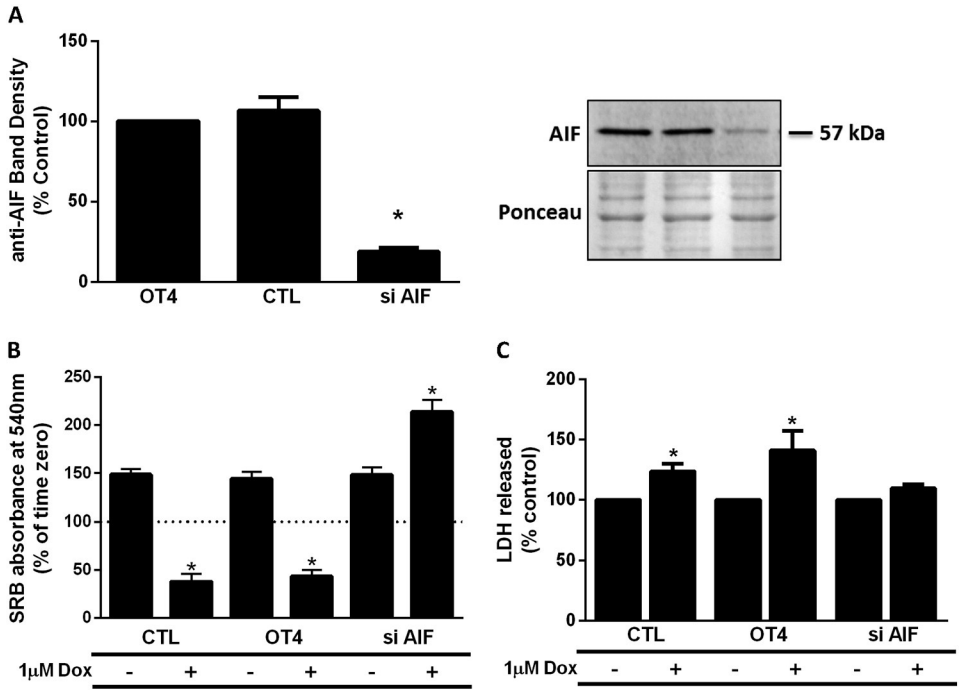

Fig. 3. AIF downregulation protects H9c2 cells from DOX toxicity. The downregulation of AIF by using siRNA was confirmed by Western Blot as a decrease in the respective band (57 kDa). A) The amount of total AIF present in control samples and in samples incubated with the non-target siRNA was equivalent. Ponceau staining shows an equal loading amount of protein in each lane. Data represent the means ± SEM of seven different experiments. *$p < 0.05$ vs OT4. B) The effect of AIF downregulation on DOX (1 μM during 48 h)-induced cell death was analyzed by using the SRB dye-binding assay. Cell treatment was performed as described in the Material and methods section. Data represent the means ± SEM of four different experiments. *$p < 0.05$ vs control (no DOX added). C) Lactate dehydrogenase assay was used to evaluate the extension of cell necrosis. The method was based in measuring LDH activity in the culture medium after DOX treatment (1 μM during 48 h). The graph represents LDH release, expressed as % of each control group. Data are expressed as mean ± SEM of eight different experiments. *$p < 0.05$ compared with the respective control.

and AIF from mitochondria, resulting in a positive feedback amplification loop [19,48]. For its release from the mitochondrial intermembrane space, AIF must be cleaved in a specific region by several proteases that may access the mitochondrial intermembrane space during an apoptotic stimulus. It is known that oxidative stress renders the AIF more susceptible to proteolytic cleavage by calpains [49]. After cleavage, truncated AIF (tAIF) is competent to execute caspase-independent apoptotic action [50,51].

Despite the essential roles of calcium and oxidative stress in AIF release from mitochondria, no study has reported the potential role of AIF in the process of DOX-dependent cardiac cell death, although the association between AIF and DOX-induced cell death has been demonstrated in cancer cells. Kim et al. measured the release of cytochrome c and AIF induced by the combination of N,N-dimethyl phytosphingosine and DOX in a variant of HL-60 cells [52]. One of the few studies that investigated the role of the AIF in a cardiac toxicity model is the work by Bae et al. [53] in which chemical inhibition of caspase activity results in a delayed release of AIF from mitochondria and induction cell death.

Our objective was thus to investigate whether DOX toxicity involves AIF release from mitochondria and its translocation to the nucleus in H9c2 cardiomyoblasts, a model for cardiac cells. This mechanism would preclude that at least an important component of DOX toxicity on this cell model results from caspase-independent apoptotic signaling. By

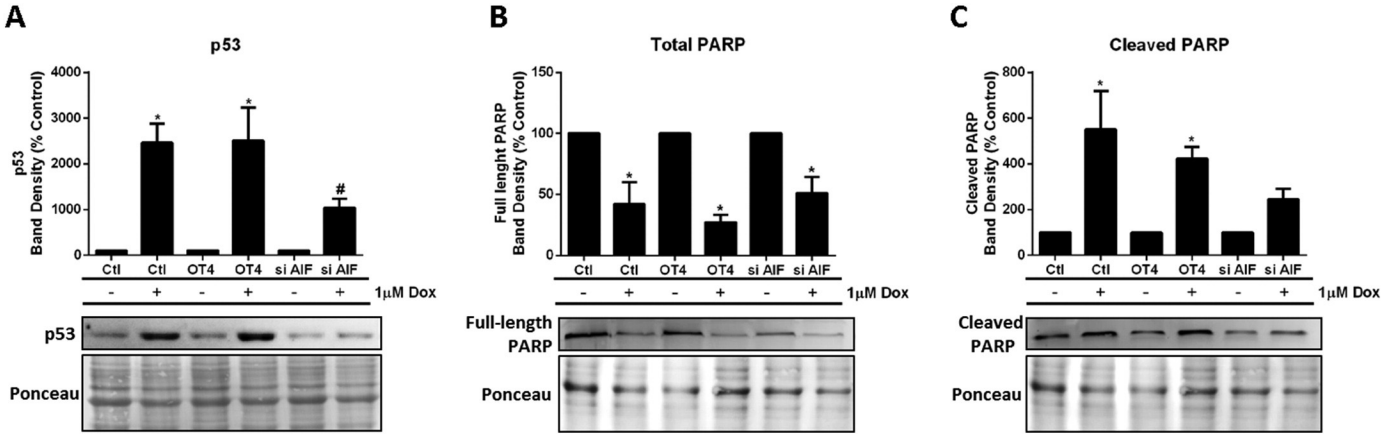

Fig. 4. AIF downregulation decreases DOX-induced p53 increase and PARP cleavage. Protein content in total cellular extracts was identified by Western Blot analysis as bands with approximately 53 (A, p53), 116 (B, full-length PARP) and 90 (C, cleaved PARP) kDa. Total cellular extracts were collected after treatment with 1 μM DOX during 48 h, as described in Material and methods section. Ponceau labeling for each Western Blotting was used as a protein loading control. The graphs represent densitometric analysis of bands, expressed as % of each control (no DOX added). Data are expressed as mean ± SEM of four different experiments for each protein. *$p < 0.05$ compared with respective control.

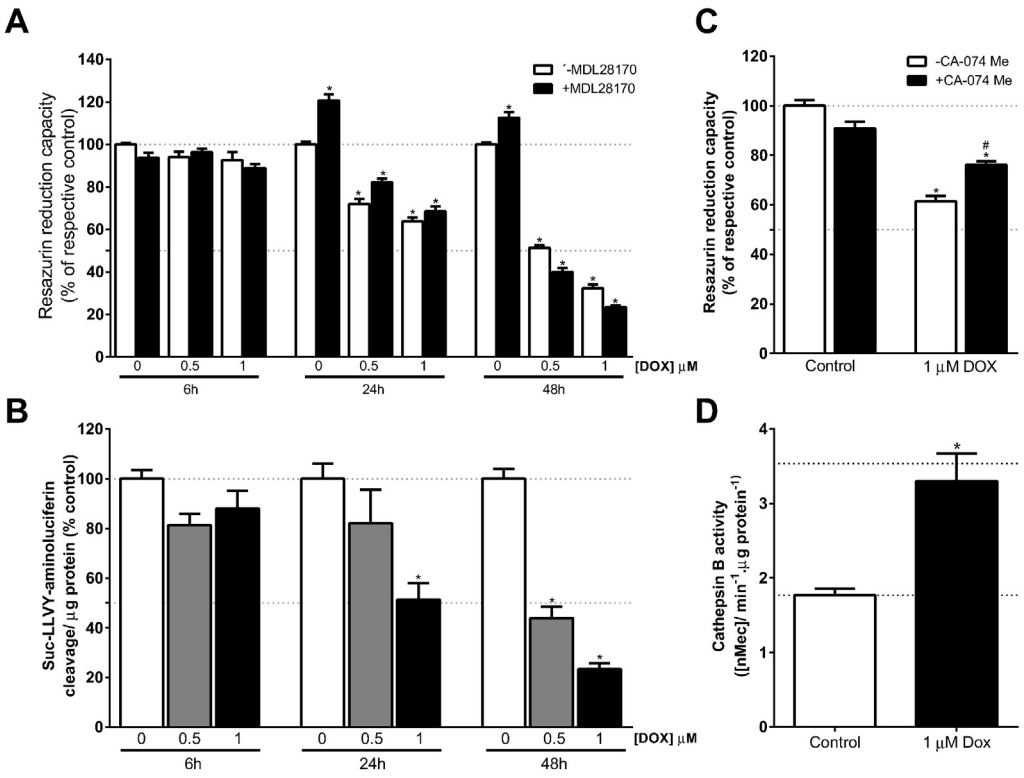

Fig. 5. DOX effects on potential AIF-cleaving proteases. DOX-induced decrease in metabolic activity was not prevented by pre-incubation with MDL28170, an unselective inhibitor of calpains (A), but the specific cathepsin B inhibitor CA-074Me was able to partially protect against DOX toxicity (C). The activity of calpains was decreased in the presence of DOX (B) but the activity of cathepsin B was increased after 24 h incubation with DOX (D). Data are expressed as mean ± SEM of four different experiments. *$p < 0.05$ compared with respective control, #$p < 0.05$ compared with DOX alone.

using Western Blotting and immunocytochemistry, AIF trafficking to the nucleus was confirmed, followed by large-scale nuclear DNA damage. AIF knockdown resulted in a decrease of DOX toxicity. The present work used H9c2 cardiomyoblasts, a commercial cell line that has been used as a model for cardiomyocytes in different studies investigating DOX toxicity [14,25–27,30]. The results obtained indicate that after 48 hour treatment with 1 μM DOX, AIF is released from mitochondria and translocated to the nuclei, where large scale 50 kbp DNA fragments were detected. The evidence that AIF actively participates on DOX-induced cell death was suggested by our silencing experiments. AIF silencing decreased DOX toxicity, including the resulting over-expression of p53 protein. This transcription factor has multiple roles within cells, including regulation of metabolism [54] and downstream pathways linking DNA damage and mitochondria-mediated cell death [55–57]. DOX toxicity is associated with redox-mediated p53 translocation to mitochondria, collaborating in the permeabilization of the outer membrane [14,58]. Several stress signals activate the p53 signaling pathway, including DNA damage, which results in p53 acetylation, enhancing its transcriptional activity [59], besides increasing the activity of PARP-1, which may also contribute to AIF release from mitochondria [60]. Our results support the idea that p53 over-expression after DOX treatment may also results from AIF-induced DNA cleavage. The protection afforded by AIF knockdown also resulted in decreased PARP cleavage, which is a caspase 3 downstream target. This fact confirms again that DOX toxicity also involves caspase activation [14,27], although the action of these proteases are not fundamental for DOX-induced cell death.

The mechanism by which AIF is released from mitochondria may be initiated through AIF cleavage by cathepsin B. In fact, pre-treatment with the cathepsin B inhibitor CA-074 Me partially protected H9c2 cells against DOX toxicity (Fig. 5C). However, it would be also expected that MDL28170, which also inhibits cathepsin B [61], would protect against DOX-induced loss of cell viability, which was not observed under our conditions (Fig. 5). This could be due to the unselective inhibition of cathepsin B, calpain-1 and calpain-2, especially because calpain-2 was reported to exert protective effects against DOX toxicity [40].

An increase in cell mass after DOX treatment in AIF-knockout cells was also observed. This result suggests that, besides leading to AIF release from mitochondria, DOX toxicity may also result from a direct interaction with AIF. In the absence of AIF, DOX treatment surprisingly resulted in increased cell proliferation. Accordingly, it was previously described that quinone compounds, including anti-cancer quinones, may prevent the accumulation of the reduced form of AIF, and enhance AIF-mediated apoptosis [62]. In addition, AIF may be responsible by the bioreductive activation of anticancer quinones, and the potentially harmful AIF-quinone interactions can be exacerbated in the presence of oxidative stress [62]. In this work, we propose a working model in which DOX toxicity causes mitochondrial ROS and loss of cytosolic calcium homeostasis, which predisposes AIF to cleavage by proteases. On the other hand, DOX direct effects on nuclear DNA result in damage which activates PARP-1 and p53, both leading to outer mitochondrial permeabilization and AIF (and cytochrome c) release. While cytochrome c release results in the activation of caspase 9 and later caspase 3, AIF translocates directly to the nuclei initiating a process of DNA cleavage which further leads to increase p53 over-expression, contributing to a positive feedback to increase mitochondrial outer membrane permeabilization (Fig. 6).

Two questions arise now. 1) Are DOX-induced AIF release and downstream caspase-independent cell death selective to the heart and 2) is this phenomenon relevant for acute, chronic or delayed DOX cardiac toxicity? As for the first question, although no experiments were performed in other cell lines, we believe that this phenomenon may occur in a much smaller scale in other tissues because of limited DOX accumulation in those tissues, as well as because of decreased DOX intra-

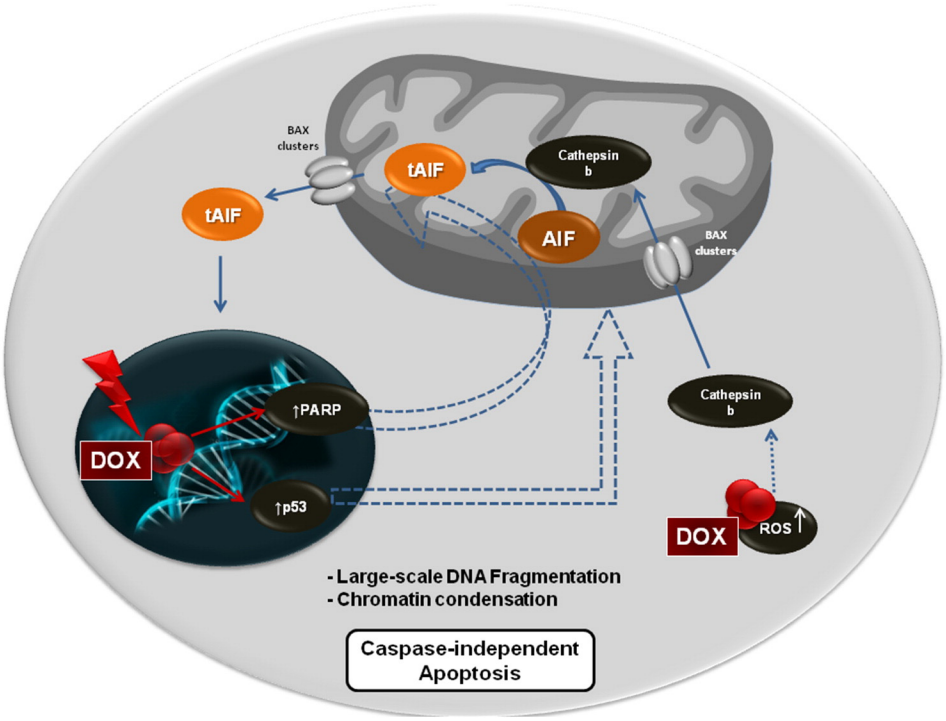

Fig. 6. New proposed mechanism of DOX-induced cardiotoxicity: schematic illustration showing our proposal for the involvement of the AIF in the mechanism of DOX-induced toxicity in H9c2 cell line. Previously we observed that DOX-induced DNA damage promoted an increase in the amount of p53 protein [14]. This increase was related with Bax clusters formation in the outer mitochondrial membrane, facilitating the release of the proapototic proteins located in the intermembrane space. In the same study we also observed that DOX-induced an increase in ROS production. Here, our results showed that DOX increases cathepsin B activity. Thus, according with the literature [67,41], and with our previous results [14], we propose that DOX-induced ROS production promotes the release of cathepsin B from lysosomes. Activated cathepsin B may gain access to the mitochondrial intermembrane space through Bax complexes in the outer mitochondrial membrane, as previously observed [14], leading to the AIF cleavage. After, truncated AIF (tAIF) is released to the cytoplasm, through the same Bax complexes, following a nuclear translocation and consequent large scale DNA fragmentation and a caspase-independent apoptosis. AIF-induced DNA damage leads further to an increase in p53 over-expression and poly(ADP-ribose) polymerase-1 (PARP1) activation, contributing to a positive feedback to increase mitochondrial outer membrane permeabilization and AIF release (more details in the Discussion section).

mitochondrial activation to a reactive semi-quinone, resulting from both lower accumulation and decreased mitochondrial activity [7]. As for the second question, the problem is actually more complex. The loss of cardiac cells due to acute DOX treatments is likely to have a role in chronic or delayed cardiac alterations because of two components. One involves the loss of cardiomyocytes and replacement by fibrotic tissue which may limit the pumping activity of the heart [63]. The second is particularly important in pediatric patients, involving selective removal of cardiac progenitors following DOX treatment, contributing to a weakening of cardiac responses to stress later in adult life [64,65]. Since H9c2 cells are cardiomyoblasts, the results here described have clinical relevance in this context, although more work must be performed in other cardiac models, including through the use of *in vivo* models.

In conclusion, the results shown here explain why anti-apoptotic strategies are not useful *per se* to counteract DOX cardiotoxicity. Instead, a multi-target strategy must be followed including the use of caspase inhibitors and mitochondrial antioxidants, besides decreasing the accumulation of DOX in non-target tissues such as the heart through liposomal carriers [66].

Supplementary data to this article can be found online at http://dx.doi.org/10.1016/j.bbadis.2014.09.015.

Disclosures

None.

Acknowledgements

This work was supported by the Portuguese Foundation for Science and Technology (FCT) research grants PTDC/SAU-TOX/117912/2010 and PTDC/DTP-FTO/1180/2012 to P.J.O. and PEst-C/SAU/LA0001/2013-2014 (from FEDER/Compete/National Budget programs) as well as by FEDER/QREN program #4832, CENTRO-07-ST24-FEDER-002008, to the CNC. The FCT also sponsored Ph.D. fellowhips SFRH/BD/33892/2009 to A.C.M. and SFRH/BD/41384/2007 to A.F.B.; V.A.S. was supported by FCT Post-doctoral fellowship SFRH/BPD/31549/2006 and afterwards by a FEDER/QREN #4832, CENTRO-07-ST24-FEDER-002008 Post-doctoral fellowship; T. C-O. was also supported by a FEDER/QREN #4832, CENTRO-07-ST24-FEDER-002008 Post-doctoral fellowship. The funding agencies had no role in the decision to publish or in the content of the manuscript. The authors are grateful to Dr Inês Araújo (University of Algarve, Portugal) for kindly providing the MDL28170 inhibitor.

References

[1] D.J. Booser, G.N. Hortobagyi, Anthracycline antibiotics in cancer therapy. Focus on drug resistance, Drugs 47 (1994) 223–258.
[2] E.N. Dessypris, D.E. Brenner, K.R. Hande, Toxicity of doxorubicin metabolites to human marrow erythroid and myeloid progenitors *in vitro*, Cancer Treat. Rep. 70 (1986) 487–490.
[3] S.M. Cutts, A. Nudelman, A. Rephaeli, D.R. Phillips, The power and potential of doxorubicin-DNA adducts, IUBMB Life 57 (2005) 73–81.
[4] J. Cummings, L. Anderson, N. Willmott, J.F. Smyth, The molecular pharmacology of doxorubicin *in vivo*, Eur. J. Cancer 27 (1991) 532–535.
[5] J.H. Doroshow, K.J. Davies, Redox cycling of anthracyclines by cardiac mitochondria. II. Formation of superoxide anion, hydrogen peroxide, and hydroxyl radical, J. Biol. Chem. 261 (1986) 3068–3074.
[6] K.J. Davies, J.H. Doroshow, Redox cycling of anthracyclines by cardiac mitochondria. I. Anthracycline radical formation by NADH dehydrogenase, J. Biol. Chem. 261 (1986) 3060–3067.
[7] F.S. Carvalho, A. Burgeiro, R. Garcia, A.J. Moreno, R.A. Carvalho, P.J. Oliveira, Doxorubicin-induced cardiotoxicity: from bioenergetic failure and cell death to cardiomyopathy, Med. Res. Rev. 34 (2013) 106–135.
[8] E. Vandecruys, V. Mondelaers, D. De Wolf, Y. Benoit, B. Suys, Late cardiotoxicity after low dose of anthracycline therapy for acute lymphoblastic leukemia in childhood, J. Cancer Surviv. 6 (2012) 95–101.

[9] S. Kumar, R. Marfatia, S. Tannenbaum, C. Yang, E. Avelar, Doxorubicin-induced cardiomyopathy 17 years after chemotherapy, Tex. Heart Inst. J. 39 (2012) 424–427.
[10] M.R. Bristow, W.A. Minobe, M.E. Billingham, J.B. Marmor, G.A. Johnson, B.M. Ishimoto, W.S. Sageman, J.R. Daniels, Anthracycline-associated cardiac and renal damage in rabbits. Evidence for mediation by vasoactive substances, Lab. Invest. 45 (1981) 157–168.
[11] M. Ueno, Y. Kakinuma, K. Yuhki, N. Murakoshi, M. Iemitsu, T. Miyauchi, I. Yamaguchi, Doxorubicin induces apoptosis by activation of caspase-3 in cultured cardiomyocytes *in vitro* and rat cardiac ventricles *in vivo*, J. Pharmacol. Sci. 101 (2006) 151–158.
[12] S.A. Susin, E. Daugas, L. Ravagnan, K. Samejima, N. Zamzami, M. Loeffler, P. Costantini, K.F. Ferri, T. Irinopoulou, M.C. Prevost, G. Brothers, T.W. Mak, J. Penninger, W.C. Earnshaw, G. Kroemer, Two distinct pathways leading to nuclear apoptosis, J. Exp. Med. 192 (2000) 571–580.
[13] Y.M. Jang, S. Kendaiah, B. Drew, T. Phillips, C. Selman, D. Julian, C. Leeuwenburgh, Doxorubicin treatment *in vivo* activates caspase-12 mediated cardiac apoptosis in both male and female rats, FEBS Lett. 577 (2004) 483–490.
[14] V.A. Sardao, P.J. Oliveira, J. Holy, C.R. Oliveira, K.B. Wallace, Doxorubicin-induced mitochondrial dysfunction is secondary to nuclear p53 activation in H9c2 cardiomyoblasts, Cancer Chemother. Pharmacol. 64 (2009) 811–827.
[15] H. Kajihara, H. Yokozaki, M. Yamahara, Y. Kadomoto, E. Tahara, Anthracycline induced myocardial damage. An analysis of 16 autopsy cases, Pathol. Res. Pract. 181 (1986) 434–441.
[16] O.J. Arola, A. Saraste, K. Pulkki, M. Kallajoki, M. Parvinen, L.M. Voipio-Pulkki, Acute doxorubicin cardiotoxicity involves cardiomyocyte apoptosis, Cancer Res. 60 (2000) 1789–1792.
[17] B.N. Bernaba, J.B. Chan, C.K. Lai, M.C. Fishbein, Pathology of late-onset anthracycline cardiomyopathy, Cardiovasc. Pathol. 19 (2010) 308–311.
[18] H.J. Youn, H.S. Kim, M.H. Jeon, J.H. Lee, Y.J. Seo, Y.J. Lee, Induction of caspase-independent apoptosis in H9c2 cardiomyocytes by adriamycin treatment, Mol. Cell. Biochem. 270 (2005) 13–19.
[19] S.A. Susin, H.K. Lorenzo, N. Zamzami, I. Marzo, B.E. Snow, G.M. Brothers, J. Mangion, E. Jacotot, P. Costantini, M. Loeffler, N. Larochette, D.R. Goodlett, R. Aebersold, D.P. Siderovski, J.M. Penninger, G. Kroemer, Molecular characterization of mitochondrial apoptosis-inducing factor, Nature 397 (1999) 441–446.
[20] I.F. Sevrioukova, Apoptosis-inducing factor: structure, function, and redox regulation, Antioxid. Redox Signal. 14 (2011) 2545–2579.
[21] E. Daugas, S.A. Susin, N. Zamzami, K.F. Ferri, T. Irinopoulou, N. Larochette, M.C. Prevost, B. Leber, D. Andrews, J. Penninger, G. Kroemer, Mitochondrio-nuclear transl ocation of AIF in apoptosis and necrosis, FASEB J. 14 (2000) 729–739.
[22] S. Landshamer, M. Hoehn, N. Barth, S. Duvezin-Caubet, G. Schwake, S. Tobaben, I. Kazhdan, B. Becattini, S. Zahler, A. Vollmar, M. Pellecchia, A. Reichert, N. Plesnila, E. Wagner, C. Culmsee, Bid-induced release of AIF from mitochondria causes immediate neuronal cell death, Cell Death Differ. 15 (2008) 1553–1563.
[23] P.S. Vosler, D. Sun, S. Wang, Y. Gao, D.B. Kintner, A.P. Signore, G. Cao, J. Chen, Calcium dysregulation induces apoptosis-inducing factor release: cross-talk between PARP-1- and calpain-signaling pathways, Exp. Neurol. 218 (2009) 213–220.
[24] L. Formentini, A. Macchiarulo, G. Cipriani, E. Camaioni, E. Rapizzi, R. Pellicciari, F. Moroni, A. Chiarugi, Poly(ADP-ribose) catabolism triggers AMP-dependent mitochondrial energy failure, J. Biol. Chem. 284 (2009) 17668–17676.
[25] V.A. Sardao, P.J. Oliveira, J. Holy, C.R. Oliveira, K.B. Wallace, Vital imaging of H9c2 myoblasts exposed to tert-butylhydroperoxide—characterization of morphological features of cell death, BMC Cell Biol. 8 (2007) 11.
[26] T. L'Ecuyer, S. Sanjeev, R. Thomas, R. Novak, L. Das, W. Campbell, R.V. Heide, DNA damage is an early event in doxorubicin-induced cardiac myocyte death, Am. J. Physiol. Heart Circ. Physiol. 291 (2006) H1273–H1280.
[27] V.A. Sardao, P.J. Oliveira, J. Holy, C.R. Oliveira, K.B. Wallace, Morphological alterations induced by doxorubicin on H9c2 myoblasts: nuclear, mitochondrial, and cytoskeletal targets, Cell Biol. Toxicol. 25 (2009) 227–243.
[28] P.J. Oliveira, J.A. Bjork, M.S. Santos, R.L. Leino, M.K. Froberg, A.J. Moreno, K.B. Wallace, Carvedilol-mediated antioxidant protection against doxorubicin-induced cardiac mitochondrial toxicity, Toxicol. Appl. Pharmacol. 200 (2004) 159–168.
[29] E.D. Danz, J. Skramsted, N. Henry, J.A. Bennett, R.S. Keller, Resveratrol prevents doxorubicin cardiotoxicity through mitochondrial stabilization and the Sirt1 pathway, Free Radic. Biol. Med. 46 (2009) 1589–1597.
[30] A.F. Branco, S.F. Sampaio, A.C. Moreira, J. Holy, K.B. Wallace, I. Baldeiras, P.J. Oliveira, V.A. Sardao, Differentiation-dependent doxorubicin toxicity on H9c2 cardiomyoblasts, Cardiovasc. Toxicol. 12 (2012) 326–340.
[31] E.C. Campos, J.L. O'Connell, L.M. Malvestio, M.M. Romano, S.G. Ramos, M.R. Celes, C.M. Prado, M.V. Simoes, M.A. Rossi, Calpain-mediated dystrophin disruption may be a potential structural culprit behind chronic doxorubicin-induced cardiomyopathy, Eur. J. Pharmacol. 670 (2011) 541–553.
[32] C.C. Lim, C. Zuppinger, X. Guo, G.M. Kuster, M. Helmes, H.M. Eppenberger, T.M. Suter, R. Liao, D.B. Sawyer, Anthracyclines induce calpain-dependent titin proteolysis and necrosis in cardiomyocytes, J. Biol. Chem. 279 (2004) 8290–8299.
[33] B.M. Frost, S. Eksborg, O. Bjork, J. Abrahamsson, M. Behrendtz, A. Castor, E. Forestier, G. Lonnerholm, Pharmacokinetics of doxorubicin in children with acute lymphoblastic leukemia: multi-institutional collaborative study, Med. Pediatr. Oncol. 38 (2002) 329–337.
[34] V. Vichai, K. Kirtikara, Sulforhodamine B colorimetric assay for cytotoxicity screening, Nat. Protoc. 1 (2006) 1112–1116.
[35] S. Wang, E.A. Konorev, S. Kotamraju, J. Joseph, S. Kalivendi, B. Kalyanaraman, Doxorubicin induces apoptosis in normal and tumor cells via distinctly different mechanisms. intermediacy of H(2)O(2)- and p53-dependent pathways, J. Biol. Chem. 279 (2004) 25535–25543.
[36] N. Yan, Y. Shi, Mechanisms of apoptosis through structural biology, Annu. Rev. Cell Dev. Biol. 21 (2005) 35–56.
[37] I. Kitazumi, M. Tsukahara, Regulation of DNA fragmentation: the role of caspases and phosphorylation, FEBS J. 278 (2011) 427–441.
[38] H. Boujrad, O. Gubkina, N. Robert, S. Krantic, S.A. Susin, AIF-mediated programmed necrosis: a highly regulated way to die, Cell Cycle 6 (2007) 2612–2619.
[39] C. Soldani, A.I. Scovassi, Poly(ADP-ribose) polymerase-1 cleavage during apoptosis: an update, Apoptosis 7 (2002) 321–328.
[40] Y. Wang, D. Zheng, M. Wei, J. Ma, Y. Yu, R. Chen, J.C. Lacefield, H. Xu, T. Peng, Overexpression of calpastatin aggravates cardiotoxicity induced by doxorubicin, Cardiovasc. Res. 98 (2013) 381–390.
[41] S. Bien, C. Rimmbach, H. Neumann, J. Niessen, E. Reimer, C.A. Ritter, D. Rosskopf, J. Cinatl, M. Michaelis, H.W. Schroeder, H.K. Kroemer, Doxorubicin-induced cell death requires cathepsin B in HeLa cells, Biochem. Pharmacol. 80 (2010) 1466–1477.
[42] H. Mizutani, S. Tada-Oikawa, Y. Hiraku, M. Kojima, S. Kawanishi, Mechanism of apoptosis induced by doxorubicin through the generation of hydrogen peroxide, Life Sci. 76 (2005) 1439–1453.
[43] S.Y. Kim, S.J. Kim, B.J. Kim, S.Y. Rah, S.M. Chung, M.J. Im, U.H. Kim, Doxorubicin-induced reactive oxygen species generation and intracellular Ca^{2+} increase are reciprocally modulated in rat cardiomyocytes, Exp. Mol. Med. 38 (2006) 535–545.
[44] Y. Kim, A.G. Ma, K. Kitta, S.N. Fitch, T. Ikeda, Y. Ihara, A.R. Simon, T. Evans, Y.J. Suzuki, Anthracycline-induced suppression of GATA-4 transcription factor: implication in the regulation of cardiac myocyte apoptosis, Mol. Pharmacol. 63 (2003) 368–377.
[45] D.L. Rigor, N. Bodyak, S. Bae, J.H. Choi, L. Zhang, D. Ter-Ovanesyan, Z. He, J.R. McMullen, T. Shioi, S. Izumo, G.L. King, P.M. Kang, Phosphoinositide 3-kinase Akt signaling pathway interacts with protein kinase Cbeta2 in the regulation of physiologic developmental hypertrophy and heart function, Am. J. Physiol. Heart Circ. Physiol. 296 (2009) H566–H572.
[46] S.A. Lipton, E. Bossy-Wetzel, Dueling activities of AIF in cell death versus survival: DNA binding and redox activity, Cell 111 (2002) 147–150.
[47] H. Ye, C. Cande, N.C. Stephanou, S. Jiang, S. Gurbuxani, N. Larochette, E. Daugas, C. Garrido, G. Kroemer, H. Wu, DNA binding is required for the apoptogenic action of apoptosis inducing factor, Nat. Struct. Biol. 9 (2002) 680–684.
[48] C. Cande, I. Cohen, E. Daugas, L. Ravagnan, N. Larochette, N. Zamzami, G. Kroemer, Apoptosis-inducing factor (AIF): a novel caspase-independent death effector released from mitochondria, Biochimie 84 (2002) 215–222.
[49] E. Norberg, V. Gogvadze, H. Vakifahmetoglu, S. Orrenius, B. Zhivotovsky, Oxidative modification sensitizes mitochondrial apoptosis-inducing factor to calpain-mediated processing, Free Radic. Biol. Med. 48 (2010) 791–797.
[50] Q. Chen, M. Paillard, L. Gomez, T. Ross, Y. Hu, A. Xu, E.J. Lesnefsky, Activation of mitochondrial mu-calpain increases AIF cleavage in cardiac mitochondria during ischemia–reperfusion, Biochem. Biophys. Res. Commun. 415 (2011) 533–538.
[51] T. Ozaki, T. Yamashita, S. Ishiguro, Mitochondrial m-calpain plays a role in the release of truncated apoptosis-inducing factor from the mitochondria, Biochim. Biophys. Acta 1793 (2009) 1848–1859.
[52] B.M. Kim, Y.J. Choi, Y.H. Lee, Y.A. Joe, S.H. Hong, N, N-Dimethyl phytosphingosine sensitizes HL-60/MX2, a multidrug-resistant variant of HL-60 cells, to doxorubicin-induced cytotoxicity through ROS-mediated release of cytochrome c and AIF, Apoptosis 15 (2010) 982–993.
[53] S. Bae, P.M. Siu, S. Choudhury, Q. Ke, J.H. Choi, Y.Y. Koh, P.M. Kang, Delayed activation of caspase-independent apoptosis during heart failure in transgenic mice overexpressing caspase inhibitor CrmA, Am. J. Physiol. Heart Circ. Physiol. 299 (2010) H1374–H1381.
[54] J. Zhuang, W. Ma, C.U. Lago, P.M. Hwang, Metabolic regulation of oxygen and redox homeostasis by p53: lessons from evolutionary biology? Free Radic. Biol. Med. 53 (2012) 1279–1285.
[55] N.D. Marchenko, A. Zaika, U.M. Moll, Death signal-induced localization of p53 protein to mitochondria. A potential role in apoptotic signaling, J. Biol. Chem. 275 (2000) 16202–16212.
[56] U.M. Moll, A. Zaika, Nuclear and mitochondrial apoptotic pathways of p53, FEBS Lett. 493 (2001) 65–69.
[57] M. Schuler, D.R. Green, Mechanisms of p53-dependent apoptosis, Biochem. Soc. Trans. 29 (2001) 684–688.
[58] R. Nithipongvanitch, W. Ittarat, M.P. Cole, J. Tangpong, D.K. Clair, T.D. Oberley, Mitochondrial and nuclear p53 localization in cardiomyocytes: redox modulation by doxorubicin (Adriamycin)? Antioxid. Redox Signal. 9 (2007) 1001–1008.
[59] N. Liu, J. Wang, R. Wang, Z. Liu, Y. Yu, H. Lu, ING5 is a Tip60 cofactor that acetylates p53 in response to DNA damage, Cancer Res. 73 (2013) 3749–3760.
[60] S.W. Yu, H. Wang, M.F. Poitras, C. Coombs, W.J. Bowers, H.J. Federoff, G.G. Poirier, T.M. Dawson, V.L. Dawson, Mediation of poly(ADP-ribose) polymerase-1-dependent cell death by apoptosis-inducing factor, Science 297 (2002) 259–263.
[61] S. Mehdi, Cell-penetrating inhibitors of calpain, Trends Biochem. Sci. 16 (1991) 150–153.
[62] L. Miseviciene, Z. Anusevicius, J. Sarlauskas, I.F. Sevrioukova, N. Cenas, Redox reactions of the FAD-containing apoptosis-inducing factor (AIF) with quinoidal xenobiotics: a mechanistic study, Arch. Biochem. Biophys. 512 (2011) 183–189.
[63] A. Goetzenich, N. Hatam, A. Zernecke, C. Weber, T. Czarnotta, R. Autschbach, S. Christiansen, Alteration of matrix metalloproteinases in selective left ventricular adriamycin-induced cardiomyopathy in the pig, J. Heart Lung Transplant. 28 (2009) 1087–1093.
[64] C. Huang, X. Zhang, J.M. Ramil, S. Rikka, L. Kim, Y. Lee, N.A. Gude, P.A. Thistlethwaite, M.A. Sussman, R.A. Gottlieb, A.B. Gustafsson, Juvenile exposure to anthracyclines impairs cardiac progenitor cell function and vascularization resulting in greater susceptibility to stress-induced myocardial injury in adult mice, Circulation 121 (2010) 675–683.
[65] A. De Angelis, E. Piegari, D. Cappetta, L. Marino, A. Filippelli, L. Berrino, J. Ferreira-Martins, H. Zheng, T. Hosoda, M. Rota, K. Urbanek, J. Kajstura, A. Leri, F. Rossi, P. Anversa, Anthracycline cardiomyopathy is mediated by depletion of the cardiac

stem cell pool and is rescued by restoration of progenitor cell function, Circulation 121 (2010) 276–292.
[66] S. Toldo, R.W. Goehe, M. Lotrionte, E. Mezzaroma, E.T. Sumner, G.G. Biondi-Zoccai, I.M. Seropian, B.W. Van Tassell, F. Loperfido, G. Palazzoni, N.F. Voelkel, A. Abbate, D.A. Gewirtz, Comparative cardiac toxicity of anthracyclines *in vitro* and *in vivo* in the mouse, PLoS One 8 (2013) e58421.
[67] L. Wang, L. Liu, Y. Shi, H. Cao, R. Chaturvedi, M.W. Calcutt, T. Hu, X. Ren, K.T. Wilson, D.B. Polk, F. Yan, Berberine induces caspase-independent cell death in colon tumor cells through activation of apoptosis-inducing factor, PLoS One 7 (2012) e36418.